Spatio-temporal characterization of ultrashort pulses diffracted by circularly symmetric hard-edge apertures: theory and experiment

Omel Mendoza-Yero,[1, 2,*] Benjamín Alonso,[3] Oscar Varela,[4] Gladys Mínguez-Vega,[1, 2] Íñigo Juan Sola,[3], Jesús Lancis,[1, 2] Vicent Climent,[1 2] and Luis Roso[4]

[1]*GROC UJI, Departament de Física, Universitat Jaume I, E12080 Castelló, Spain.*
[2]*Institut de Noves Tecnologies de la Imatge (INIT), Universitat Jaume I, E 12080 Castelló, Spain.*
[3]*Departamento de Física Aplicada, Universidad de Salamanca E-37008 Salamanca, Spain.*
[4]*Centro de Láseres Pulsados, CLPU, E-37008 Salamanca, Spain.*
**omendoza@fca.uji.es*

Abstract: We carry out a complete spatio-temporal characterization of the electric field of an ultrashort laser pulse after passing through a diffractive optical element composed of several binary amplitude concentric rings. Analytical expressions for the total diffraction field in the time and spectral domain are provided, using the Rayleigh-Sommerfeld formulation of the diffraction. These expressions are experimentally validated. The spatio-temporal amplitude and phase structure of the pulse are measured at different planes beyond the diffractive optical element using spatially-resolved spectral interferometry assisted by an optical fiber coupler (STARFISH). Our results allow corroborating theoretical predictions on the presence of multiple pulses or complex spectral distributions due to the diffraction-induced effects by the hard-edge ring apertures.

OCIS codes: (260.1960) Diffraction theory; (320.2250) Femtosecond phenomena, (320.7100) Ultrafast Measurements.

References and links

1. M. Lefrançois, and S. F. Pereira, "Time evolution of the diffraction pattern of an ultrashort laser pulse," Opt. Express **11**(10), 1114–1122 (2003).
2. Z. Jiang, R. Jacquemin, and W. Eberhardt, "Time dependence of Fresnel diffraction of ultrashort laser pulses by a circular aperture," Appl. Opt. **36**(19), 4358–4361 (1997).
3. J. Li, H. Zhang, D. R. Alexander, D. W. Doerr, and N. R. Tadepalli, "Diffraction characteristics of 10fs laser pulses passing through an aperture," J. Opt. Soc. Am. A **22**(7), 1304–1310 (2005).
4. H. E. Hwang, G. H. Yang, and P. Han, "Near-field diffraction characteristics of a time-dependence Gaussian-shape pulsed beam from a circular aperture," Opt. Eng. **42**(3), 686–695 (2003).
5. O. Mendoza-Yero, G. Mínguez-Vega, J. Lancis, M. Fernández-Alonso, and V. Climent, "On-axis diffraction of an ultrashort light pulse by circularly symmetric hard apertures," Opt. Express **15**(8), 4546–4556 (2007).
6. Z. L. Horváth, and Z. Bor, "Diffraction of short pulses with boundary diffraction wave theory," Phys. Rev. E Stat. Nonlin. Soft Matter Phys. **63**(2), 026601 (2001).
7. Z. Liu, and B. Lü, "Spectral shifts and spectral switches in diffraction of ultrashort pulsed beams passing through a circular aperture," Optik (Stuttg.) **115**(10), 447–454 (2004).
8. M. Gu, and X. S. Gan, "Fresnel diffraction by circular and serrated apertures illuminated with an ultrashort pulsed-laser beam," J. Opt. Soc. Am. A **13**(4), 771–778 (1996).
9. R. Netz, and T. Feurer, "Diffraction of ultrashort laser pulses and applications for measuring pulse front distortion and pulse width," Appl. Phys. B **70**, 813–819 (2000).
10. S. P. Veetil, N. K. Viswanathan, C. Vijayan, and F. Wyrowski, "Spectral and temporal evolutions of ultrashort pulses diffracted through a slit near phase singularities," Appl. Phys. Lett. **89**(4), 041119 (2006).
11. H. Zhang, J. Li, D. W. Doerr, and D. R. Alexander, "Diffraction characteristics of a Fresnel zone plate illuminated by 10 fs laser pulses," Appl. Opt. **45**(33), 8541–8546 (2006).
12. C. J. Zapata-Rodríguez, "Temporal effects in ultrashort pulsed beams focused by planar diffracting elements," J. Opt. Soc. Am. A **23**(9), 2335–2341 (2006).
13. R. Ashman, and M. Gu, "Effect of ultrashort pulsed illumination on foci caused by a Fresnel zone plate," Appl. Opt. **42**(10), 1852–1855 (2003).
14. J. Pearce, and D. Mittleman, "Defining the Fresnel zone for broadband radiation," Phys. Rev. E Stat. Nonlin. Soft Matter Phys. **66**(5), 056602 (2002).

#130847 - $15.00 USD Received 29 Jun 2010; revised 5 Aug 2010; accepted 7 Aug 2010; published 17 Sep 2010

15. O. Mendoza-Yero, G. Mínguez-Vega, J. Lancis, and V. Climent, "Focusing and spectral characteristics of periodic diffractive optical elements with circular symmetry under femtosecond pulsed illumination," J. Opt. Soc. Am. A **24**(11), 3600–3605 (2007).
16. O. Mendoza-Yero, G. Mínguez-Vega, J. Lancis, E. Tajahuerce, and V. Climent, "Spectral analysis of femtosecond pulse diffraction through binary diffractive optical elements: theory and experiment," Opt. Express **16**(4), 2541–2546 (2008).
17. M. Born, and E. Wolf, *Principles of Optics*, 7th ed. (Cambridge University press, 2005).
18. G. Mínguez-Vega, O. Mendoza-Yero, J. Lancis, and V. Climent, "Proposal for the generation of THz bursts and codes of shaped femtosecond pulses using binary mask," IEEE Photon. Technol. Lett. **19**(21), 1732–1734 (2007).
19. B. Xia, L. R. Chen, P. Dumais, and C. L. Callender, "Ultrafast pulse train generation with binary code patterns using planar lightwave circuits," Electron. Lett. **42**(19), 1119–1120 (2006).
20. S. A. Ponomarenko, and E. Wolf, "Spectral anomalies in a Fraunhofer diffraction pattern," Opt. Lett. **27**(14), 1211–1213 (2002).
21. X. Hu, and J. Pu, "Spectral anomalies of polychromatic, spatially coherent light diffracted by an annular apertures in the far field," Chin. Opt. Lett. **3**, 418–421 (2005).
22. J. Pu, C. Cai, and S. Nemoto, "Spectral anomalies in Young's double-slit interference experiment," Opt. Express **12**(21), 5131–5139 (2004).
23. C. Dorrer, E. M. Kosik, and I. A. Walmsley, "Direct space time-characterization of the electric fields of ultrashort optical pulses," Opt. Lett. **27**(7), 548–550 (2002).
24. D. J. Kane, and R. Trebino, "Characterization of Arbitrary Femtosecond Pulses Using Frequency-Resolved Optical Gating," IEEE J. Quantum Electron. **29**(2), 571–579 (1993).
25. C. Iaconis, and I. A. Walmsley, "Spectral phase interferometry for direct electric-field reconstruction of ultrashort optical pulses," Opt. Lett. **23**(10), 792–794 (1998).
26. P. Gabolde, and R. Trebino, "Single-shot measurement of the full spatio-temporal field of ultrashort pulses with multi-spectral digital holography," Opt. Express **14**(23), 11460–11467 (2006).
27. P. Bowlan, P. Gabolde, and R. Trebino, "Directly measuring the spatio-temporal electric field of focusing ultrashort pulses," Opt. Express **15**(16), 10219–10230 (2007).
28. P. Bowlan, U. Fuchs, R. Trebino, and U. D. Zeitner, "Measuring the spatiotemporal electric field of tightly focused ultrashort pulses with sub-micron spatial resolution," Opt. Express **16**(18), 13663–13675 (2008).
29. F. Bonaretti, D. Faccio, M. Clerici, J. Biegert, and P. Di Trapani, "Spatiotemporal amplitude and phase retrieval of Bessel-X pulses using a Hartmann-Shack sensor," Opt. Express **17**(12), 9804–9809 (2009).
30. P. Saari, P. Bowlan, H. Valtna-Lukner, M. Lõhmus, P. Piksarv, and R. Trebino, "Basic diffraction phenomena in time domain," Opt. Express **18**(11), 11083–11088 (2010).
31. B. Alonso, Í. J. Sola, Ó. Varela, J. Hernández-Toro, C. Méndez, J. San Román, A. Zaïr, and L. Roso, "Spatiotemporal amplitude-and-phase reconstruction by Fourier-transform of interference spectra of high-complex-beams," J. Opt. Soc. Am. B **27**(5), 933–940 (2010).
32. L. Lepetit, G. Cheriaux, and M. Joffre, "Linear techniques of phase measurement by femtosecond spectral interferometry for applications in spectroscopy," J. Opt. Soc. Am. B **12**(12), 2467–2474 (1995).

1. Introduction

The latest advances in our understanding fundamental physical phenomena on the diffraction of ultrashort laser pulses by hard-edge apertures open the way to the use of diffractive optical elements (DOEs) as a tool for controlling the spatial and temporal features of light pulses. In this context, there has been a growing interest in studying diffraction-induced effects due to propagating ultrashort laser pulses through binary amplitude DOEs. Several recent works have addressed the study of the spectral and temporal characteristics of ultrashort laser pulses diffracted by a circular aperture [1–7], serrated apertures [8], single and double slits [9,10], Fresnel zone plates [11–14], or DOEs having multiple rings [15,16]. Because in most cases the analysis was performed within the spectral or the temporal domain separately, the diffraction effects on the incident ultrashort pulse were understood independently.

In the time domain, the shape of the temporal profiles at a given output plane can be determined from the coherent superposition of geometric and boundary wave pulses [6,17]. In accordance with the Miyamoto-Wolf theory of the boundary diffraction wave, the boundary wave pulse describes a disturbance emerging from the points of the edge of an aperture, whereas the geometric pulse represents a wave governed by the laws of geometrical optics [6]. Taking advantage of this fact, it is possible not only to characterize the temporal evolution of diffracted pulses [1–6], but also to split the incident ultrashort pulse in a train of pulses of different peak heights, modify the temporal shape of the instantaneous intensity or vary its temporal width, in a controllable manner [18]. Such a temporal manipulation of ultrashort laser pulses can produce binary code patterns that might be used, for instance, as optical

#130847 - $15.00 USD Received 29 Jun 2010; revised 5 Aug 2010; accepted 7 Aug 2010; published 17 Sep 2010

packet-headers in packet-switched networks and for photonically assisted generation of microwave and millimeter waveforms [19].

In the spectral domain, the total diffracted field is assessed by the sum of all field contributions due to the different spectral components of the pulse by means of e.g. the Huygens-Fresnel integral, among other methods. Then, the square modulus of the total diffracted field expressed as a wavelength-dependent function can be thought as a spectral modifier of the spectrum corresponding to the incident pulse. That is, at a given spatial coordinate after the DOE the resultant spectral power is calculated from the multiplication of the spectral modifier by the corresponding spectral power of the incident pulse. The above relationship was applied to investigate the diffraction of a spatially coherent, polychromatic wave at a circular aperture [20], an annular aperture [21] or double slits [22], which showed that drastic spectral changes take place near a phase singularity. At such a point, the intensity of the diffracted field has a zero value, the phase becomes indeterminate and the field in the neighborhood has a complex structure exhibiting dislocation and vortices. Regarding this topic, Ponomarenko and Wolf pointed out that spectral shifts toward blue and red directions of the spectrum could be associated with different bits of information that can be transmitted over appreciable distances, suggesting its use in free-space communication applications [20]. Also, in the framework of the Rayleigh-Sommerfeld formulation of the diffraction, different changes in the spectrum of a femtosecond pulse originated by diffraction of an ultrashort laser pulse through a hard-edge aperture consisting of circularly symmetric transparent rings have been reported [16]. In this work it was shown that spectral changes (i.e., split and/or shift of the spectrum) in the vicinity of a spectral anomaly or in focal positions can occur as well. Note that the possibility of manipulating the output spectrum of an ultrashort pulse by means of a suitable DOE design finds application in material processing, ultrafast spectroscopy and/or photochemistry.

However, when space-time coupling occurs one cannot assume that the temporal and spatial characteristics of a short pulse are independent [23]. In fact, in most nonlinear interactions or focusing processes in ultrafast optics, there is some coupling between the space and time features of the pulse. For a binary amplitude DOE having several rings, the spatio-temporal coupling can appear while focusing the electric field associated with an ultrashort pulse along the optical axis. In this case, a characterization of the diffracted field cannot be detached from the spatio-temporal analysis.

In this manuscript, we provide an analytical approach for the spatiotemporal characterization of the electric field of an ultrashort pulse after propagation through any circularly symmetric binary amplitude DOE. The physical model is developed in the framework of the Rayleigh-Sommerfeld theory of the diffraction, allowing us to compute the spatio-temporal behavior of the diffracted field both for the on-axis and the off-axis cases. The theoretical results are corroborated by experiments. At this point, since there is a marked spatio-temporal coupling, traditional methods to measure the temporal profile of short pulses on axis (e.g. FROG [24] or SPIDER [25]) or only their spatial profile and wave-front are not enough. To this end, other methods have been recently developed, such as STRIPED FISH [26], SEA TADPOLE [27], [28] or Shackled-FROG [29]. For instance, by using SEA TADPOLE technique the evolution and interference of the boundary waves behind an opaque disk and also behind a circular opening has been experimentally demonstrated [30]. In the present work, the spatio-temporal coupled amplitude and phase of the diffracted pulse is measured at different transversal planes from the DOE using a recently developed method. It consists of spatially resolved spectral interferometry assisted by a fiber coupler interferometer (STARFISH) [31], also obtaining the spatially resolved spectrum structure. The spatial resolution of our technique allows characterizing the spatio-temporal field structure in and near the axial foci of the DOE.

2. Analytical approach

Suppose we have a circularly symmetric hard aperture consisting of N transparent rings, with N an integer positive number, illuminated by an ultrashort laser pulse. The pulse can be

#130847 - $15.00 USD Received 29 Jun 2010; revised 5 Aug 2010; accepted 7 Aug 2010; published 17 Sep 2010

considered as a set of monochromatic plane waves with various frequencies, propagating in the same direction. The polar coordinates r,θ are assumed at the input plane, whereas for any parallel output plane, located at a distance z from the aperture, corresponding coordinates R,ϕ are used. With the help of the first Rayleigh-Sommerfeld diffraction integral an approximate analytical expression for the field, $U_m(z,R,\omega)$, diffracted from the edge of a ring under plane wave illumination can be obtained as [16]

$$U_m(z,R,\omega) \approx U_{im}(z,R,\omega) - U_{om}(z,R,\omega) \tag{1}$$

Where,

$$U_{im/om}(z,R,\omega) = \frac{z\exp\left(i\frac{\omega}{c}\sqrt{z^2+r_{im/om}^2}\right)J_0\left(\frac{\omega}{c}\frac{r_{im/om}R}{\sqrt{z^2+r_{im/om}^2}}\right)}{\sqrt{z^2+r_{im/om}^2}} \tag{2}$$

In Eq. (2), r_{im} and r_{om} are respectively the inner and the outer radii of the m-th transparent ring and ω is a frequency component of the pulse. The term $J_0(\xi)$ denotes the Bessel function of the first kind with zero order and argument ξ. For the on-axis case ($R=0$), Eq. (1) provides the exact solution for the diffracted field, see Appendix A of [5]. In the off-axis region, it holds for points several hundreds of microns away from the propagation axis [16]. From the superposition principle, the total diffraction field $U(z,R,\omega)$ is assessed by the sum of the contributions from each transparent ring, $U(z,R,\omega) = \sum_{m=1}^{N} U_m(z,R,\omega)$. Hence, the power spectrum $S(z,R,\omega)$ at points onto the output plane in the vicinity of the optical axis can be determined by the well-known expression [20–22]

$$S(z,R,\omega) = S_0(\omega)\left|U(z,R,\omega)\right|^2 \tag{3}$$

In Eq. (3), $S_0(\omega)$ is the power spectrum of the incident pulse. It is apparent that using Eq. (3) one can study the diffraction-induced spectral changes associated with an ultrashort pulse after propagation through the above DOE. That is, for an arbitrary point located at the output plane $z = z_1$ with coordinates z_1, R_1, the function $\left|U(z_1,R_1,\omega)\right|^2$ modifies the power spectrum of the incident pulse accordingly. In addition, by numerically solving the integral $\int S(z,R,\omega)d\omega$ over the bandwidth of the pulse, spatial broadening effects in the irradiance pattern can be also investigated [14,15]. Therefore, Eq. (3) allows us to characterize both the spectral and focusing behavior of circularly symmetric binary DOEs under pulsed illumination [15,16].

Based on Eq. (1) we derive an analytical expression for the total diffraction field, $U_{time}(z,R,t)$, in the time domain. To do that, the spatio-temporal coupling of the field due to the frequency-dependent diffracted field is taken into account by means of the following inverse Fourier transform

$$U_{time}(z,R,t) = \frac{1}{2\pi}\int_{-\infty}^{\infty} A(\omega)U(z,R,\omega)\exp(-i\omega t)d\omega \tag{4}$$

#130847 - $15.00 USD Received 29 Jun 2010; revised 5 Aug 2010; accepted 7 Aug 2010; published 17 Sep 2010

The term $A(\omega)$ is the spectral amplitude of the incident pulse ($S_0(\omega)=|A(\omega)|^2$), which is related to the temporal amplitude of the same pulse, $u(t)$, by the Fourier transform

$$A(\omega)=\int_{-\infty}^{\infty}u(t)\exp(i\omega t)dt \tag{5}$$

After substituting corresponding expressions for $U(z,R,\omega)$ and $A(\omega)$ into Eq. (4), and carrying out some mathematical manipulations, one can obtain the following expression

$$U_{time}(z,R,t)=\sum_{m=1}^{N}F_{im}(z,R,t)-F_{om}(z,R,t) \tag{6}$$

Where,

$$F_{im/om}(z,R,t)=\frac{z}{\sqrt{z^2+r_{im/om}^2}}\frac{1}{2\pi}\int_0^{2\pi}u\left(t-\frac{\sqrt{z^2+r_{im/om}^2}}{c}+\frac{r_{im/om}R\cos\theta}{c\sqrt{z^2+r_{im/om}^2}}\right)d\theta \tag{7}$$

The Eq. (6) is the main analytical result of this manuscript. It is derived within the framework of the Rayleigh-Sommerfeld theory of diffraction. Equation (6) holds for points not only on-axis but also in the close vicinity of the propagation axis. In particular, the validity of Eq. (6) for points 200 μm away from the propagation axis will be experimentally demonstrated in section 5. In determining Eq. (6) no paraxial approximation was assumed, so it can be applied as well in near or far field regions. After a visual inspection of Eq. (6) and (7), one sees that the total diffraction field $U_{time}(r,R,t)$ is given by the sum of $2N$ boundary wave pulses coming from the edges of the transparent rings. In the particular case of having a central transparent zone ($r_{i1}=0$) a geometric wave pulse appears, consequently $F_{i1}(z,R,t)=u(t-z/c)$. Apart from the weighting factor $z/(z^2+r_{im/om}^2)^{1/2}$, the field amplitude of the boundary wave pulses is equal to that of the incident pulse $u(t)$. However, due to the dependence of the argument ξ in the function $u(\xi)$ on the coordinates z, R and radii $r_{im/om}$, the boundary wave pulses do not arrive at the same time to the output plane. At this point, the term $(z^2+r_{im/om}^2)^{1/2}/c$ is the propagation time for a pulse that travels from the inner or outer edge of the m-th annular aperture to the on-axis point at the output plane z. Starting from the same origin, the propagation time to get to an off-axis point ($R\neq 0$) is approximately determined by adding to the first term a second one given by $r_{im/om}R\cos\theta/[c(z^2+r_{im/om}^2)^{1/2}]$ in the argument of the function $u(\xi)$. Note that the azimuthal average through the angle θ takes into account propagation times lower and greater than $(z^2+r_{im/om}^2)^{1/2}/c$ because of the factor $\cos\theta$. This corresponds with the fact that for off-axis points the circular symmetry is lost. In particular, when $R=0$, Eq. (6) reduces to the exact solution of the Rayleigh-Sommerfeld on-axis diffraction integral for an ultrashort light pulse diffracted by circularly symmetric hard apertures [5]. In this case, it is easy to see that the propagation time difference among boundary wave pulses decreases when increasing the distance between the output plane and the DOE. From the argument of $u(\xi)$ it is also apparent that the phase of the boundary wave pulses varies with the propagation distance z. In addition, the sum in Eq. (6) indicates that there is a phase difference of π between two boundary wave pulses originated at certain ring aperture.

#130847 - $15.00 USD Received 29 Jun 2010; revised 5 Aug 2010; accepted 7 Aug 2010; published 17 Sep 2010

3. Spatio-temporal simulations

We consider an incident plane-wave pulse with temporal amplitude given by $u(t)=\exp(-i\omega_0 t)\exp[-t^2/(4\sigma^2)]$, where ω_0 reads for the carrier frequency of the pulse and σ represents its standard deviation width. In this case, the integral term $F_{im/om}(z,R,t)$ can be expressed in the form

$$F_{im/om}(z,R,t)=\frac{z\exp\left[-i\omega_0\left(t-\frac{s_{im/om}}{c}\right)\right]}{s_{im/om}}\exp\left[-\frac{\left(t-\frac{s_{im/om}}{c}\right)^2}{4\sigma^2}\right]J_0\left(\omega_0\frac{r_{im/om}R}{cs_{im/om}}\right) \quad (8)$$

Where $s_{im/om}=\sqrt{z^2+r_{im/om}^2}$ is the distance between the inner or outer edge of the m-th annular aperture and the on-axis point at the output plane z. To obtain Eq. (8) we assume that $1+z^2/r^2 >> R/r\cos\theta$ in the pulse envelope term $\exp[-t^2/(4\sigma^2)]$. This assumption is fulfilled for any set of parameters z, $r=r_{im/om}$ and θ, if the values of R are small enough. Consequently, we focus our attention on points in the neighborhood of the propagation axis. For most practical applications the above approach is useful because the energy due to diffraction is concentrated very close to the z axis.

On the other hand, we select a DOE periodic in the squared radial coordinate in which the ratio between the areas of the whole period and its transparent part is a positive integer number ε. Note that in the case of $\varepsilon=2$ the areas of opaque and transparent regions are equal which coincides with the well-known Fresnel zone plate. The on-axis focusing and spectral characteristics of optical elements having $\varepsilon\neq 2$ under ultrashort illumination have been investigated [15]. According to previous results, we know that inner and outer radii of these optical elements can be determined by the expressions: $r_{im}=[p(m-1)]^{1/2}$ and $r_{om}=[p(m-(1-1/\varepsilon))]^{1/2}$, respectively.

To illustrate the spatio-temporal behavior of the diffracted pulses we made three movies of the time evolution of the instantaneous intensity $\left|U_{time}(z,R,t)\right|^2$ at different z, R intervals, always corresponding to spatial regions in the vicinity of the propagation axis. These intervals within the near field, Fig. 1(a), Fresnel, Fig. 1(b), and far-field, Fig. 1(c) regions, allow us to better understand the interaction process that takes place among boundary wave pulses. Regarding this aspect, it is convenient to recall that the temporal shape of the instantaneous intensity depends on the distance from the diffractive aperture [5]. The main reason for that is the interference among boundary wave pulses during propagation.

In the paraxial approximation, the axial location of the above regions can be estimated. Within this approach, the time difference between two boundary wave pulses coming from the edges of an aperture Δt_1 or from neighboring apertures Δt_2 can be calculated, yielding $\Delta t_1 = p/(2\varepsilon cz)$ and $\Delta t_2 = p(\varepsilon-1)/(2c\varepsilon z)$, respectively. Besides, owing to the fact that for $R=0$ Gaussian functions $\left|F_{im/om}(z,0,t)\right|$ never fully decay, a criterion for pulse proximity without significant interaction is needed. At this point, we assume 2σ as the minimum time difference to fulfill this criterion. Therefore, the near field region $z < p/(4c\varepsilon\sigma)$ can be determined by the condition $\Delta t_1 > 2\sigma$, the Fresnel region $p/(4c\varepsilon\sigma)\le z\le p(\varepsilon-1)/(4c\varepsilon\sigma)$ by $\Delta t_1\le 2\sigma$ and $\Delta t_2\ge 2\sigma$, whereas the far-field region $z > p(\varepsilon-1)/(4c\varepsilon\sigma)$ by $\Delta t_2 < 2\sigma$. For the present study the incident ultrashort pulse is characterized by $\omega_0 = 2.37\times10^{15}$ Hz corresponding to a central wavelength of 795 nm, and $\sigma = 12.7$ fs to an intensity full width at

#130847 - $15.00 USD Received 29 Jun 2010; revised 5 Aug 2010; accepted 7 Aug 2010; published 17 Sep 2010

half maximum of 30 fs. In addition, the design parameters of the DOE were $N = 10$, $\varepsilon = 4$ and $p = 3.2\ mm^2$. In accordance with the above parameters, one can realize that the DOE is made up of ten transparent rings, such that the smallest ring radius is $r_{i1} = 0$ and the largest one is $r_{o10} = 5.4\ mm$. In addition, the ring widths in the squared radial coordinate are the same ($r_{om}^2 - r_{im}^2 = p/\varepsilon = 0.8\ mm^2$). It can be also verified that above defined regions are found at $z < 52.3$ mm (near-field region), $52.3\ \text{mm} \le z \le 157.0\ \text{mm}$ (Fresnel region) and $z > 157.0$ mm (far-field region).

To compare the transverse extension of the diffracted pulses at different regions, the sampling interval of R is fixed to $[-20\mu m,\ 20\mu m]$ for all movies. In Fig. 1(a), the axial interval was limited to $z \in [34.980\ \text{mm}\ 35.020\ \text{mm}]$. In this case, the time difference among boundary wave pulses does not allow significant interaction. So, in the near field the instantaneous intensity is composed of one pulse per circular hard edge ($2N$ pulses). Note that, due to the central transparent zone of the mask, the first pulse corresponds to the geometric wave pulse. In the second movie shown in Fig. 1(b), the axial interval is defined as $z \in [140.980\ \text{mm}\ 141.020\ \text{mm}]$. Within this interval, the time difference Δt_1 has decreased and the pairs of two boundary wave pulses coming from inner and outer edges of each transparent ring do interact (Fresnel region). The coherent interference of these pulses determines the temporal profile of the resulting burst. Depending on the phase difference, the temporal profile can be a set of N single lobes with an inward central ripple, Gaussian-like form or flattop profiles [5]. The movie shown in Fig. 1(b) corresponds to the Fresnel region. In this case, the instantaneous intensity is made up of a burst of N pulses having Gaussian-like structure, instead of $2N$ pulses as before. Here it should be recalled that the filling ratio $\varepsilon \neq 2$ does not allow equal transparent and opaque portions within a period of the mask, but the transparent area is lower than the opaque one. Therefore, two pulses originated at a given transparent ring of the mask meet before two pulses emitted at different ring apertures. In the far-field region, Δt_2 is also lower enough to cause the interaction of all pulses of the burst. In this region, the temporal profile will depend again on the phase difference among pulses. For instance, in Fig. 1(c) corresponding to an axial interval $z \in [202.980\ \text{mm}\ 203.020\ \text{mm}]$ the temporal profile has flattop shape. However, due to the coherent interference among pulses, other temporal profiles are possible, e.g. a set of N Gaussian-like pulses. As far as the distance from the mask is further increased, the temporal profile of the instantaneous intensity approaches to that of the incident pulse.

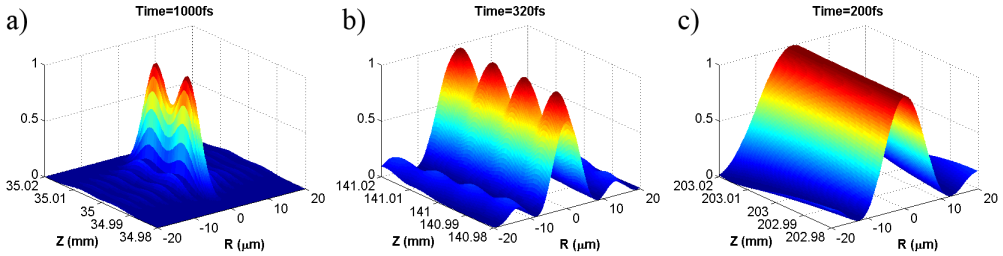

Fig. 1. Movies of the spatio-temporal time evolution of the instantaneous intensity at different spatial regions a) (2.02 MB Media 1) Near-field region, b) (0.77 MB Media 2) Fresnel region, and c) (0.57 MB Media 3) Far-field region.

4. Experimental setup

To check the validity of our theoretical model, we performed measurements of the spatio-temporal amplitude and phase after the DOE. For the experiments, we have used a CPA Ti: Sapphire laser (from Amplitude Systems), delivering 30 fs (FWHM) pulses centered at 795

#130847 - $15.00 USD Received 29 Jun 2010; revised 5 Aug 2010; accepted 7 Aug 2010; published 17 Sep 2010

nm. The energy we used was low (less than 100 μJ), obtained from attenuation of the beam with a variable attenuator (a half-wave plate and a linear polarizer before the CPA compressor) and some neutral density filters, in order to perform measurement in linear regime. The laser beam passed through a beam splitter plate: the transmitted beam acted as reference beam, while the reflected one illuminates the DOE, creating the test pulse.

The test pulse was characterized by means of Spatio-Temporal Amplitude-and-phase Reconstruction by Fourier-transform of Interference Spectra of High-complex-beams STARFISH [31]. This reconstruction technique consists of spatially resolved spectral interferometry using an optical fiber coupler as interferometer. The experimental setup is shown in Fig. 2. The reference and the test beam are collected by each fiber input port. The test arm spatially scans the transverse profile and the reference arm controls the relative delay between the pulses required for the interferometry (between 2 and 3 ps in the experimental conditions of the present study). Both pulses are combined inside the fiber coupler and leave it through the output common port that is directly connected to a standard spectrometer (from Avantes), where the interference spectra are measured. Notice that this scheme does not require collinear test and reference, avoiding the precise alignment of the beams. Also, the reference beam is not scanned and its spectral phase is obtained on-axis just by means of a SPIDER measurement (from APE). The control of the longitudinal position of the DOE allows scanning different propagation distances.

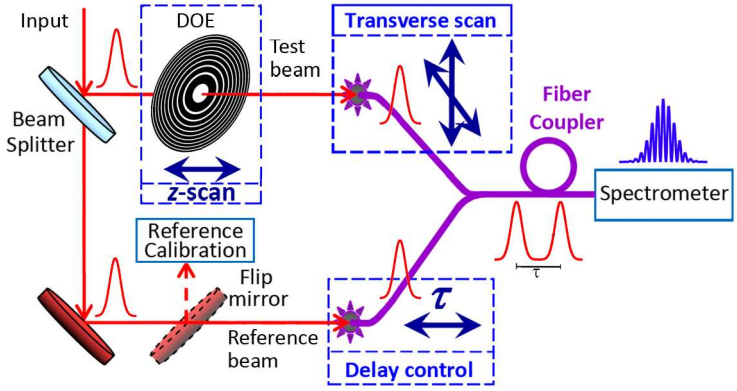

Fig. 2. Experimental setup: one replica of the laser pulse is used as the reference and the other replica illuminates the DOE (test beam). The pulses are collected by the arms of the fiber coupler, the reference one controls the relative delay, whereas the test one spatially scans the test beam. The spatially resolved SI is measured after the fiber coupler in the spectrometer. The position of the DOE allows exploring different propagation distances.

The fiber coupler must be single mode for the whole spectral range, in order to prevent pulse distortions. In our case, it means a 4 μm mode field diameter, which gives us a high spatial resolution. The two arms of the fiber coupler should have equal length. Slight phase differences were calibrated and taken into account through a single spectral interferometry measurement using the same input pulse at both fiber ports.

To reconstruct the test pulse, the information of the spectral interferences is used to obtain the spectral phase difference between both pulses (reference and test) by applying the fringes inversion algorithm known as Fourier-Transform Spectral Interferometry (FTSI) [32]. Since the reference is calibrated with SPIDER, it allows obtaining the spectral phase of the test pulse. This information is combined with a separate scan for the test spectrum measurement (collecting only the test pulse with the reference blocked), and it is equivalent to the knowledge of the temporal amplitude and phase of the test pulse by doing the inverse Fourier-transform. The extension to spatial domain is achieved by the transverse scan of the test fiber port, thus constituting the full characterization of the spatio-temporal (and spatio-spectral) amplitude and phase of the beam at certain propagation distance. The spatio-temporal coupling is preserved in the measurement because the reference is kept constant, what allows

#130847 - $15.00 USD Received 29 Jun 2010; revised 5 Aug 2010; accepted 7 Aug 2010; published 17 Sep 2010

measuring test pulse front structure. In our case, the system presents cylindrical symmetry, so we have only scanned in one transverse direction (*x*-axis), therefore obtaining a reconstruction along the radial coordinate.

For the experiment we select three transverse planes located within the near-field, Fresnel and far-field regions defined in the previous section. These are those corresponding to the axial positions $z = 35$ mm , $z = 141$ mm and $z = 203$ mm . Note that the above planes are included within the axial sections selected for the movies in section 3. Figure 3 shows the on-axis irradiance $I(z,\omega_0)$ for the central wavelength of the pulse. With the help of Eq. (3), $I(z,\omega_0)$ can be derived from the integral $I(z,\omega) = \int_0^\infty S(z,0,\omega)d\omega$, after setting $R = 0$ and $\omega = \omega_0$. Note that for the monochromatic case $\omega = \omega_0$, the power spectrum of the incident pulse $S_0(\omega)$ can be expressed as a Dirac function. Under ultrashort pulsed illumination, the on-axis irradiance $I(z,\omega_0)$ gives us a rough estimation of the foci distribution after the DOE. The exact irradiance distribution $I(z,\omega)$ must be numerically calculated using the above integral. In Fig. 3, the axial positions of the experimental planes are indicated. The position of the first experimental plane, which is located very close to the DOE, was represented alone in left part of Fig. 3, because it needs quite more sampling than the last two. In addition, a smoothing function was applied in Fig. 3 left. For each plane, several spatio-temporal reconstructions have been done in order to obtain an accurate description of the light behavior.

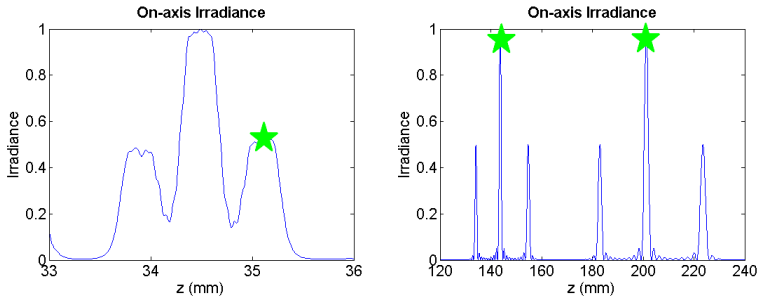

Fig. 3. On-axis irradiance pattern of the DOE for the central wavelength of the pulse. The green stars correspond approximately to the positions of the spatio-temporal reconstructed planes at *z* = 35mm, *z* = 141mm and z = 203mm shown later in Fig. 4, 5 and 6, respectively.

5. Experimental results

In Figs. 4-6, the experimental results are shown and compared with the theoretical simulations (analytical), corresponding to propagation distances 35 mm, 141 mm and 203 mm. In all cases, the theoretical simulations of spatially resolved spectra are shown in subfigures (a), meanwhile the spatio-temporal intensity of the pulses in subfigures (b). These figures are compared with the corresponding experimental results given in subfigures (c) for experimental spatially resolved spectra, and in subfigures (d) for experimental time evolution of the pulses.

In particular, the spatio-temporal structure for the axial position $z = 35$ mm after the DOE is shown in Fig. 4. There is a very structured spectrum, presenting some sharp peaks. Its dependence with the transverse coordinate corresponds to a complex spatio-temporal distribution of the beam. In the spatio-temporal domain, each par of two pulses of the train, slightly distinguished from the theoretical curve in Fig. 4(b), has approximately 90 fs intensity FHWM with a time distance of 150 fs among them. As commented in section 3, this is the expected behavior in the near field region, see Fig. 1(a) and movie 1. In the experiment, certain pairs of two pulses are poorly visible and some times do not appear. For instance, in Fig. 4(d) the contributions to the diffracted field of the geometric wave pulse (direct pulse) and the first-arrival boundary wave pulse are indistinguishable. Here, it can be mentioned that

#130847 - $15.00 USD Received 29 Jun 2010; revised 5 Aug 2010; accepted 7 Aug 2010; published 17 Sep 2010

in Fig. 3 of reference [30], recorded by SEA TADPOLE technique and corresponding to the spatio-temporal electric field distribution after the diffraction of a short pulse by a circular hole, both contributions do not overlap.

The measurement at the plane $z = 35$ mm , which is very close to the DOE, is difficult to accomplish due to the low diffraction energy at the given focus and its small spatial width. In addition, it presents another problem: the numerical aperture (NA) of the optical fiber limits the coupling of the light for tight-focusing conditions. In this case, taking into account the NA provided by the fiber's manufacturer (NA = 0.11 ± 0.01) and the design parameters of the DOE, it can be shown that the number of rings allowed by the NA condition is between 4 (for NA = 0.10) and 6 (NA = 0.12). Accordingly, Fig. 4(d) clearly shows four axial pair of two pulses. Therefore, in the particular conditions given at the plane $z = 35$ mm , our measurement does not have enough spatial resolution to resolve all pulses within the train. Note that those pulses propagating at angles larger than the NA of the fiber do not appear in Fig. 4(d). One solution for this problem is given in [28], where Bowlan and associates use near-field scanning microscopy probes for improving the performance of the SEA TADPOLE technique. Despite of the above-mentioned problem, it is possible to observe a reasonable good agreement between theory and experiment in the forward part of the spatio-temporal structure. Others discrepancies may come from the assumption of plane-wave illumination and the used of an ideal Gaussian spectral distribution. The inclusion of a Gaussian illumination or the experimental pulsed light spectrum into the theoretical model implies numerical calculus and so, no longer analytical solutions.

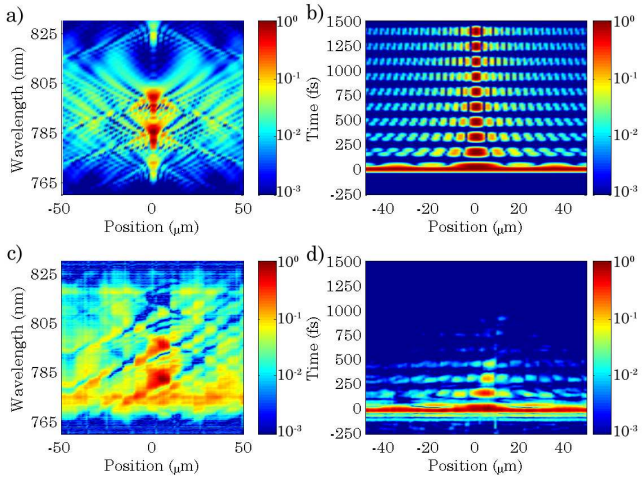

Fig. 4. Simulated and experimental spatially resolved spectrum (a, c), and corresponding spatio-temporal intensity (b, d) for the propagation distance z = 35mm.

In Fig. 5, the complex structure observed in Fig. 4 remains when the focus at position $z = 141$ mm is analyzed. The measurements are very symmetric with respect to the center in the radial direction. The spatially resolved theoretical and experimental spectra in Fig. 5(a) and 5(c), show a maximum located within 10 μm around the optical axis. The off-axis spectral contribution appears in a structured way. This is translated to the spatio-temporal field as a complex distribution (Fig. 5(b), theoretical and 5(d), experimental), presenting a train of 10 pulses (one per ring of the mask) of about 16 fs intensity FWHM and 38 fs from peak to peak. Off-axis the different pulses forming the train after the main peak front exhibit divergent structure. The agreement between simulation and theory is notable.

#130847 - $15.00 USD Received 29 Jun 2010; revised 5 Aug 2010; accepted 7 Aug 2010; published 17 Sep 2010

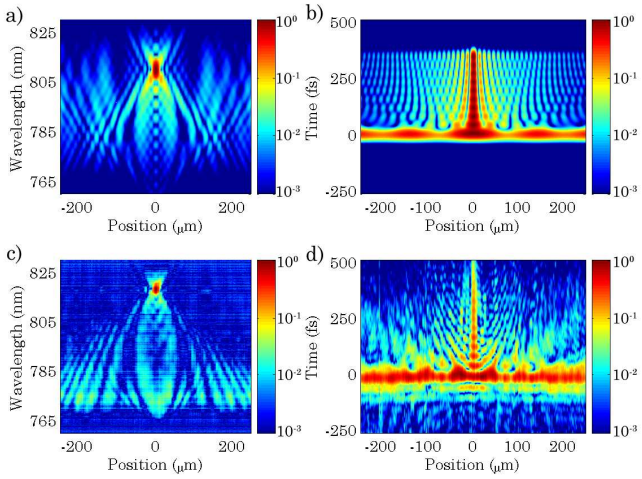

Fig. 5. Simulated and experimental spatially resolved spectrum (a, c), corresponding spatio-temporal intensity (b, d) for the propagation distance z = 141mm.

The characteristics of the pulse at the plane $z = 203$ mm are shown in Fig. 6. Here, some features observed for the plane $z = 141$ mm remain, while important differences appear. In the spatio-spectral domain, a main central peak and the wings are still observed presenting x-shape, as seen in Fig. 6(a) and (c). In the spatio-temporal domain shown in Fig. 6(b) and (d), the pulses from the former train (see Fig. 4 and 5) now merge into a broad central pulse of 250 fs intensity FWHM, shorter than the former pulse train, but longer than the input pulse. Off-axis, it is possible to see a wing structure, still preserving the train pulse structure. This behavior is caused by the lower angle of the light converging to this longer focus, since the time difference between the central and the outermost rings of the DOE is reduced.

Finally, it should be pointed out that in comparison with the theoretical spatio-temporal distributions, experimental results given in Fig. 4(d), 5(d) and 6(d) show a slightly temporal pulse broadening. We believe that this is mainly caused by dispersion of the short pulse while passing through the DOE material (quartz).

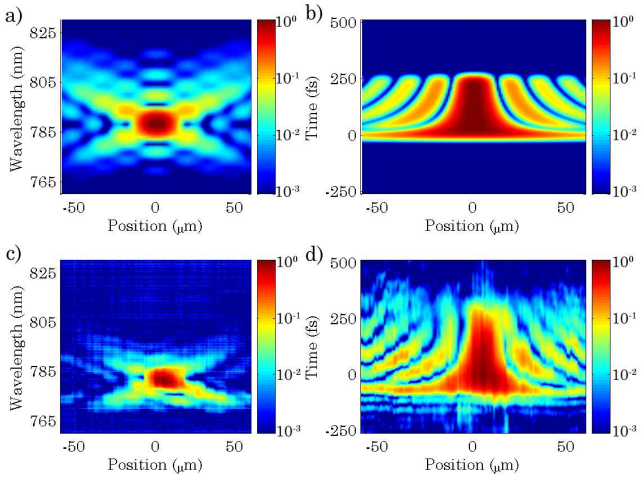

Fig. 6. Simulated and experimental spatially resolved spectrum (a, c), corresponding spatio temporal intensity (b, d) for the propagation distance z = 203mm.

#130847 - $15.00 USD Received 29 Jun 2010; revised 5 Aug 2010; accepted 7 Aug 2010; published 17 Sep 2010

6. Conclusions

A physical model based on Rayleigh-Sommerfeld theory of diffraction useful for studying the pass of an ultrashort pulse by any circularly symmetric amplitude DOE has been developed. It contains analytical expressions that allow for a fast and accurate description of the diffraction phenomenon both in the spatio-spectral and spatio-temporal domains. Full experimental reconstructions of spatio-spectral and spatio-temporal field distribution at different propagation positions have been carried out with fiber coupler spectral interferometry (STARFISH). The results of measurements showed the complex spatio-temporal structure of the field near several foci of the DOE, observing different behaviors for the near, Fresnel and far-field regions. The agreement between theory and experiment is quite good.

Acknowledgements

We acknowledge support from Spanish Ministerio de Ciencia e Innovación through the Consolider Program SAUUL (CSD2007-00013) and Research projects FIS2009-09522 and FIS2010-15746, from Junta de Castilla y León through the Program for Groups of Excellence (GR27) and from the EC's Seventh Framework Programme (LASERLAB-EUROPE, grant agreement n° 228334). We also acknowledge support from the Centro de Laseres Pulsados, CLPU, Salamanca, Spain. B. Alonso and I. J. Sola acknowledge the support from the Spanish Ministerio de Ciencia e Innovación through the "Formación de Profesorado Universitario" and "Ramón y Cajal" grant programs respectively.

#130847 - $15.00 USD Received 29 Jun 2010; revised 5 Aug 2010; accepted 7 Aug 2010; published 17 Sep 2010